Simultaneous Modification of Alumina and $MgO{\cdot}Al_2O_3$ Inclusions by Calcium Treatment During Electroslag Remelting of Stainless Tool Steel

CHENG-BIN SHI, WEN-TAO YU, HAO WANG, JING LI, and MIN JIANG

Calcium modification of both alumina and $MgO{\cdot}Al_2O_3$ inclusions during protective gas electroslag remelting (P-ESR) of 8Cr17MoV stainless steel and its effect on nitrides and primary carbides were studied by analyzing the transient evolution of oxide and sulfide inclusions in the P-ESR process. The oxide inclusions that were not removed during P-ESR without calcium treatment were found to retain their original state until in as-cast ingot. Calcium treatment modified all $MgO{\cdot}Al_2O_3$ and alumina inclusions that had not been removed in the P-ESR process to liquid/partially liquid $CaO\text{-}Al_2O_3\text{-}(MgO)$ with uniformly distributed elements, in addition to a small proportion of partially modified inclusions of a $CaO\text{-}MgO\text{-}Al_2O_3$ core surrounded by a liquid $CaO\text{-}Al_2O_3$. The modification of low-MgO-containing $MgO{\cdot}Al_2O_3$ inclusions involves the preferential reduction of MgO from the $MgO{\cdot}Al_2O_3$ inclusion by calcium and the reaction of calcium with Al_2O_3 in the inclusion. It is the incomplete/complete reduction of MgO from the spinel by calcium that contributes to the modification of spinels. Alumina inclusions were liquefied by direct reaction with calcium. Calcium treatment during P-ESR refining also provided an effective approach to prevent the formation of nitrides and primary carbides in stainless steel through modifying their preferred nucleation sites (alumina and $MgO{\cdot}Al_2O_3$ inclusions) to calcium aluminates, which made no contribution to improving the steel cleanliness.

DOI: 10.1007/s11663-016-0771-1

I. INTRODUCTION

In recent years, the increasing demand for more excellent properties of engineering component materials and tool steels (such as automobile engine components, razor blades, and knives) has led to the development of new martensitic stainless steel grades with higher carbon content in view of their higher hardness. Electroslag remelting (ESR) refining is widely used in the production of these high-grade steels. To improve steel cleanliness, deoxidation of liquid steel with aluminum is generally employed in producing electrode steel for ESR, consequently generating endogenous Al_2O_3 and $MgO{\cdot}Al_2O_3$ inclusions in aluminum-killed steel.[1,2] Unfortunately, it is a fact that original oxide inclusions in electrode can hardly be removed completely through ESR practice even if particular efforts are made such as optimization of slag chemistry and/or melt rate.

These nondeformable oxide inclusions often act as breakage initiation sites during rolling (0.7 mm in thickness of rolled sheet) and specific machining of these high-carbon steels, as well as seriously degrade the surface quality, toughness, and fatigue behaviors of stainless tool steel products.[3–6] Moreover, Al_2O_3 and $MgO{\cdot}Al_2O_3$ inclusions could also provide heterogeneous nucleation sites for primary carbides and nitrides in these high-carbon steels, promoting their formation,[7–9] which inevitably leads to similar detriments as alumina and $MgO{\cdot}Al_2O_3$ inclusions to the subsequent deformation processing and properties of tool steels,[3,6,10] and so do nitrides.

Modifying oxide inclusions to a lower melting-point state, which corresponds to pronounced deformability, is an alternative countermeasure to minimize their detriments to steel,[11–16] except for maximizing inclusion removal during liquid steel refining. Calcium modification of alumina and spinel inclusions in industrial refining practice[1,17–24] and laboratory experiments[1,25–27] has been investigated by many researchers, and they proposed various modification routes (even controversial viewpoints). These previous studies[1,17–27] have confirmed that the effectiveness and routes of calcium modification are determined by various factors, such as slag and steel chemistry, reaction reactor types, and refining operation.

ESR differs greatly from other refining technologies in practical operation and refining principle. However, control of oxide inclusions by calcium treatment during ESR has not been studied yet, except the earlier work by one of the present authors.[28] It has been proven that although the original inclusions in electrodes are calcium aluminates, the remaining inclusions are

CHENG-BIN SHI, Assistant Professor, WEN-TAO YU, and HAO WANG, Ph.D. Students, JING LI, Professor, and MIN JIANG, Assistant Professor, are with the State Key Laboratory of Advanced Metallurgy, University of Science and Technology Beijing (USTB), Beijing 100083, P.R. China. Contact e-mail: chengbin.shi@ustb.edu.cn
Manuscript submitted January 30, 2016.
Article published online August 29, 2016.

$MgO{\cdot}Al_2O_3$ spinels in remelted steel after ESR.[29] This suggests that modification of high-melting-point oxide inclusions during ESR to less harmful ones is more effective than inclusions control in the process of electrode steel production.

Magnesium-alumina spinels are a solid solution between $MgAl_2O_4$ and Al_2O_3. In the spinels, the solid solution extends from 16.2 mass pct of MgO to 28.2 mass pct of MgO at 1873 K (1600 °C).[30,31] Even though one of the current authors' work[28] has confirmed that spinels could be modified readily by calcium during the ESR process to low-melting-point calcium aluminates. There is still a lack of systematical study regarding alumina and low-MgO inclusions modification by calcium during the ESR process and its comparison with that in other refining practices. The current work was motivated to address the issues as follows:

1. The possibility and mechanism of calcium modification of low-MgO $MgO{\cdot}Al_2O_3$ inclusions during ESR refining (herein these inclusions are not always spinels). (Previous work indicated that it was because of the preferential reduction of MgO from the spinel by calcium that the modification of spinels to calcium aluminates could be achieved.[1,20] Whether calcium could remarkably modify low-MgO inclusions and a similar mechanism held as that in modification of spinels reported by Shi *et al.*[28] and other researchers[1,20] is still not clear.)
2. The possible extent of alumina inclusions modification by calcium during ESR refining in the case where both alumina and $MgO{\cdot}Al_2O_3$ inclusions coexist in electrode steel. (Previous studies showed an opposite opinion on whether alumina or spinel is easier to be modified.[4,23,32])
3. The role of CaS formation in modification of alumina and $MgO{\cdot}Al_2O_3$ inclusions in aluminum-killed steel with high-sulfur content. (Previous studies demonstrated that the modification of alumina and spinel inclusions proceeded through transient CaS formation immediately after calcium injection into aluminum-killed steel containing 40 to 100 ppm sulfur.[1,26,27])

II. EXPERIMENTAL

A. *ESR Experimental Procedure*

High-carbon martensitic stainless steel 8Cr17MoV is typically produced as follows: induction furnace melting → LF refining → horizontal continuous casting → ESR → hot rolling → pickling → cold rolling. A 8Cr17MoV steel rod with a diameter of 90 mm was used as a consumable electrode in P-ESR experiments. The chemical composition of the consumable electrode is listed in Table I. The premelted slag (29.3 mass pct CaF_2, 30.5 mass pct CaO, 34.5 mass pct Al_2O_3, 3.8 mass pct MgO, 1.9 mass pct SiO_2) was roasted at 973 K (700 °C) in an electrical resistance furnace for 8 hours to remove the moisture in the slag before P-ESR experiments.

The schematic diagram of the P-ESR apparatus has been illustrated in a previous publication.[28] The inner diameter of a water-cooled copper mold is 170 mm. The oxide scale on the electrode steel surface was basically removed mechanically prior to ESR experiments. In the case of calcium treatment, calcium wire (calcium metal purity 97.8 pct, 7 mm in diameter) enclosed in a seamless steel tube (1.5 mm in thickness) that attached to an electrode was continuously added as the electrode was inserted downward during ongoing ESR. The detailed descriptions of the alloy addition technique have been presented elsewhere.[33] The first trial T1 was performed without calcium addition. The calcium wires addition was 9 and 18 kg/t of steel in trials T2 and T3, respectively.

The operating current, voltage, and outlet temperature of the mold cooling water were maintained at about 2800 A, 45 V, and 313 K (40 °C) in each P-ESR trial, respectively. The melt rate was approximately 75 kg/h in each trial. The remelting was conducted under the atmosphere of argon gas at a gas flow rate of 20 NL/min in the whole ESR procedure. A steel sample was taken from a liquid metal pool in mold during P-ESR refining using a vacuum sampling tube that was made of quartz (6 mm in inner diameter), followed by quenched in water to examine inclusions evolution in this refining process. The sampling from a liquid metal pool was performed at the time when about two thirds of the whole refining process was finished. The as-cast ingots produced in trials T1, T2, and T3 were designated as ESR-1, ESR-2, and ESR-3, respectively. The height of as-cast ingot is about 250 mm.

B. *Chemical Analysis and Microscopic Observation*

The inductively coupled plasma atomic emission spectroscopy (ICP-AES) was performed to analyze the contents of soluble Al, Ca, Mg, Si, Mn, Cr, Ni, Mo, V, and Ti in consumable electrode, and the contents of soluble Al, Ca, and Mg in remelted ingots. The total oxygen, sulfur, and carbon contents in the steel were measured by the inert gas fusion-infrared absorptiometry. The nitrogen content was determined by an inert gas fusion-thermal conductivity method. The chemical analysis was performed at the National Analysis Center for Iron and Steel, China.

A metallographic sample was taken from the mid-height of each as-cast ESR ingot at the mid-radius position. Steel samples were mechanically polished by silicon carbide papers and diamond paste for analyzing inclusion characteristics by scanning electron microscope (SEM, FEI Quanta-250; FEI Corporation, Hillsboro, OR) equipped with an energy-dispersive X-ray spectrometer (EDS, XFlash 5030; Bruker, Germany). The instrument was operated at an acceleration voltage of 20 kV.

The cross section of metallographic sample was etched with a solution of 25-mL alcohol, 25-mL hydrochloric acid, and 5-g ferric chloride for a few seconds at room temperature, and then it was examined by SEM–EDS again to observe its microstructure.

To reveal the transient evolution of inclusions in the ESR process, the steel samples that were collected from the liquid metal pool by vacuum sampling tubes were mounted with epoxy resin, polished, and then examined by SEM–EDS to observe inclusion characteristics.

III. RESULTS AND DISCUSSION

A. *Remelted Ingot Composition*

The chemical compositions of electroslag remelted ingots are listed in Table II. It is clear that calcium addition did not apparently reduce the oxygen and sulfur contents further in ESR refining, indicating an invalid role of calcium in improving steel cleanliness. The total oxygen content, as a general criterion to assess steel cleanliness, decreases from 58 ppm in the electrode to 40 ppm in remelted ingot. The decrease in sulfur content from 64 ppm in the electrode to around 24 ppm in remelted ingots demonstrated noticeable desulfurization of the current ESR trials.

The magnesium content maintains 4 ppm regardless of calcium treatment in the ESR process. The decrease in the total magnesium content in steel after P-ESR provided an evidence of considerable removal of original $MgO{\cdot}Al_2O_3$ inclusions, whereas the inclusion removal through P-ESR is still in a limited extent. Calcium content in the steel shows a slight increase with increasing calcium addition. The aluminum content increases from 0.058 mass pct in the electrode to 0.089 mass pct in remelted ingots with increasing calcium addition during the P-ESR process. This constant aluminum pickup is considered to result from calcium wires that usually contain aluminum as an impurity, as well as originate from the reaction between calcium and alumina in molten slag, as expressed in the following equation:[34]

$$\begin{aligned} &3[Ca] + (Al_2O_3) = 2[Al] + 3(CaO) \\ &\Delta G_1^\circ = -733500 + 59.7T(J/mol) \end{aligned} \quad [1]$$

Thermodynamically, the aluminum pickup that arises from the reaction between calcium and alumina inclusions is more likely due to the higher Al_2O_3 activity in alumina inclusions compared with that in molten slag. However, the quantitative calculation showed that the maximum limit of aluminum pickup according to this reaction is 0.0065 mass pct assuming that all oxygen in steel existed as alumina inclusions. Compared with the measured values shown in Table II, it can be obtained that this reaction has a negligible contribution to aluminum pickup.

B. *Characteristics of Inclusions and Primary Carbides*

1. *Inclusions in consumable electrode*

From SEM–EDS determination, the oxide inclusions in the consumable electrode were identified as either Al_2O_3 or $MgO{\cdot}Al_2O_3$ inclusions. Figure 1 presents the SEM backscattered electron (BSE) images and EDS results of typical inclusions in the electrode. The SEM–EDS analysis revealed that the observed $MgO{\cdot}Al_2O_3$ inclusions could be categorized into two types according to the height of Mg peak of EDS spectra, and the composition of these inclusions was quite uniform. One is pure spinels ($MgAl_2O_4$-Al_2O_3 solid solutions) in Figures 1(c), (d), and (h). The other is low-MgO-containing (<10 mass pct of MgO) inclusions [with compositions in the spinel + alumina two-phase region at 1873 K (1600 °C)][1] as shown in Figures 1(e) and (f). Similar observations were also reported by Verma *et al.* in aluminum-killed steel.[1] It is noted that all observed oxide inclusions are irregular in morphology and mostly about 1 to 4 μm in size. Most of these oxide inclusions were observed to be partially surrounded by a manganese sulfide inclusion (see Figure 1). The SEM micrograph and element mappings of typical dual-phased inclusions are presented in Figure 2. The obtained results showed that the majority of manganese sulfide inclusions were adhering to oxide inclusions and that pure manganese sulfide inclusions were just occasionally found.

2. *Inclusions and primary carbides in remelted ingots*

In the case of remelting without calcium treatment, all oxide inclusions were identified as alumina or $MgO{\cdot}Al_2O_3$ in ingot ESR-1. The BSE images and EDS results of typical inclusions in ingot ESR-1 are shown in Figure 3. Most of these oxide inclusions serve as a nucleation site for nitride (Ti,V)N formation. Pure alumina and $MgO{\cdot}Al_2O_3$ inclusions were just occasionally found. No single-phased nitrides (without oxide inclusion core) were observed. It should be mentioned that the majority of these dual-phased precipitates

Table I. Chemical Composition of the Consumable Electrode Used in P-ESR Experiments (Mass Pct)

C	Si	Mn	Cr	Ni	Mo	V	Ca	Mg	Ti	Al	S	N	O
0.89	0.66	0.49	17.16	0.19	1.05	0.12	<0.0005	0.0007	0.013	0.058	0.0064	0.032	0.0058

Table II. Chemical Compositions of Remelted Ingots (Mass Pct)

Ingot No.	O	Al	Ca	Mg	N	S
ESR-1	0.0040	0.053	<0.0005	0.0004	0.031	0.0025
ESR-2	0.0046	0.075	0.0005	0.0004	0.035	0.0024
ESR-3	0.0040	0.089	0.0009	0.0005	0.035	0.0022

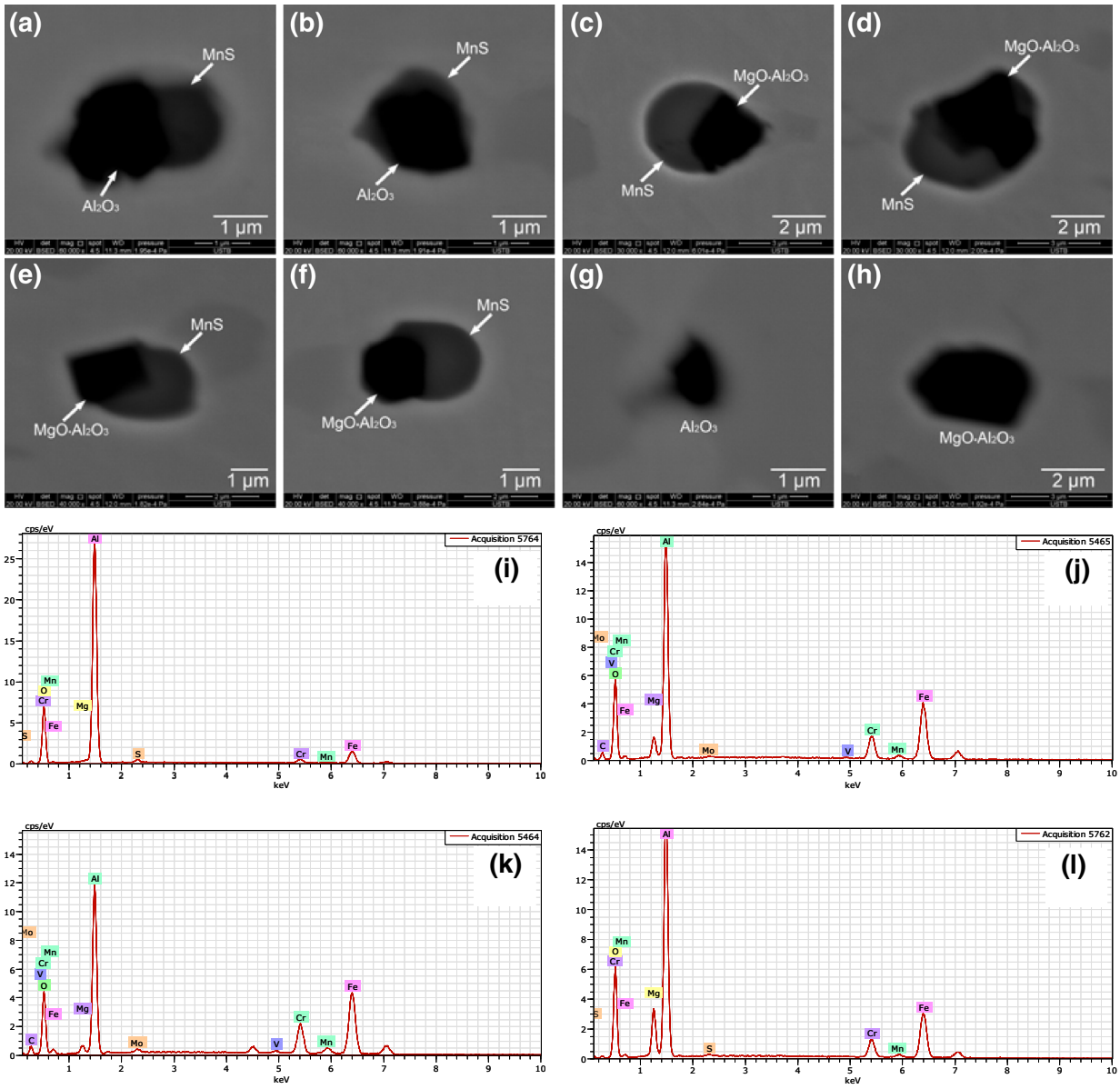

Fig. 1—Typical original inclusions in the consumable electrode. (EDS spectrums shown in (*i*), (*j*), (*k*), and (*l*) correspond to the oxide inclusions shown in (*a*), (*e*), (*f*), and (*h*), respectively.).

seemed likely to act as a nucleation site for primary carbides (see Figures 4(a) and (d)). Meanwhile, there are a large amount of primary carbides without heterogeneous nucleation core as shown in Figures 4(e) and (f).

In P-ESR refining, calcium treatment did change the compositions of original inclusions considerably. The element mappings of typical inclusions observed in ingot ESR-2 are illustrated in Figure 5. The oxide inclusions in the ingot are mainly partially modified inclusions of a $CaO-MgO-Al_2O_3$ core surrounded by an outer $CaO-Al_2O_3$ layer, together with occasionally observed inclusions of an unreacted Al_2O_3 core surrounded by a $CaO-Al_2O_3$ layer (see Figure 5(b)), which is an indication of incomplete modification by calcium. Another kind of dual-phased $CaO-MgO-Al_2O_3$ + $CaO-Al_2O_3$ inclusion was also occasionally found. In these inclusions, the Al concentration is inhomogeneous throughout their cross sections (an example is shown in Figure 5(e)). A portion containing Mg of the inclusion is higher in Al and lower in Ca, whereas the other portion (Mg-free region) is lower in Al and higher in Ca.

A large amount of $CaO-MgO-Al_2O_3$ inclusions containing a very small amount of MgO and $CaO-Al_2O_3$ inclusions, both of which were homogeneous in compositions, was also found in ingot ESR-2 as shown in Figures 5(a), (c), and 6(a). Two examples of partially extracted inclusions in ingot are shown in Figure 6. The partially modified $MgO{\cdot}Al_2O_3$ inclusions are featured with the enrichment of CaO in the MgO-poor region. It is clear that the fully and partially calcium-modified

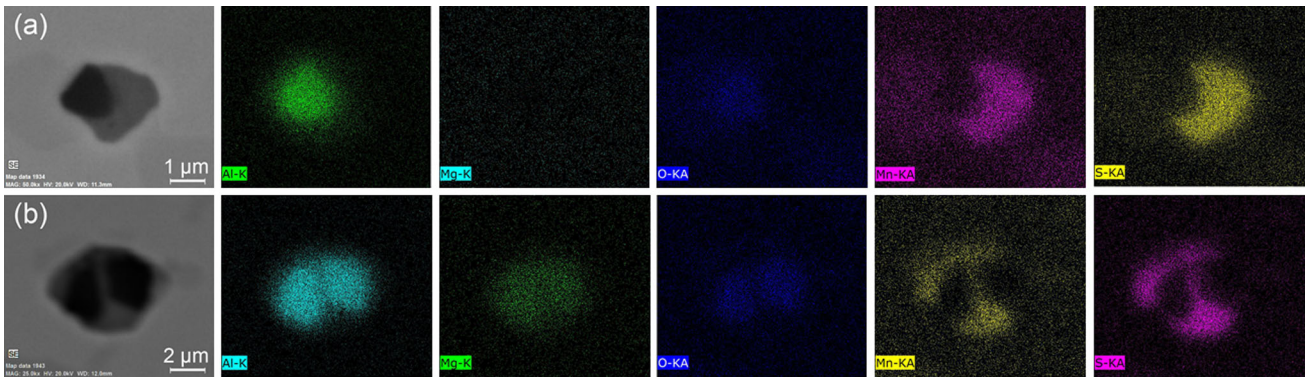

Fig. 2—Element mappings of typical dual-phased inclusions in consumable electrode: (*a*) MnS adhering to alumina and (*b*) dual-phased inclusion of $MgO{\cdot}Al_2O_3$ + MnS.

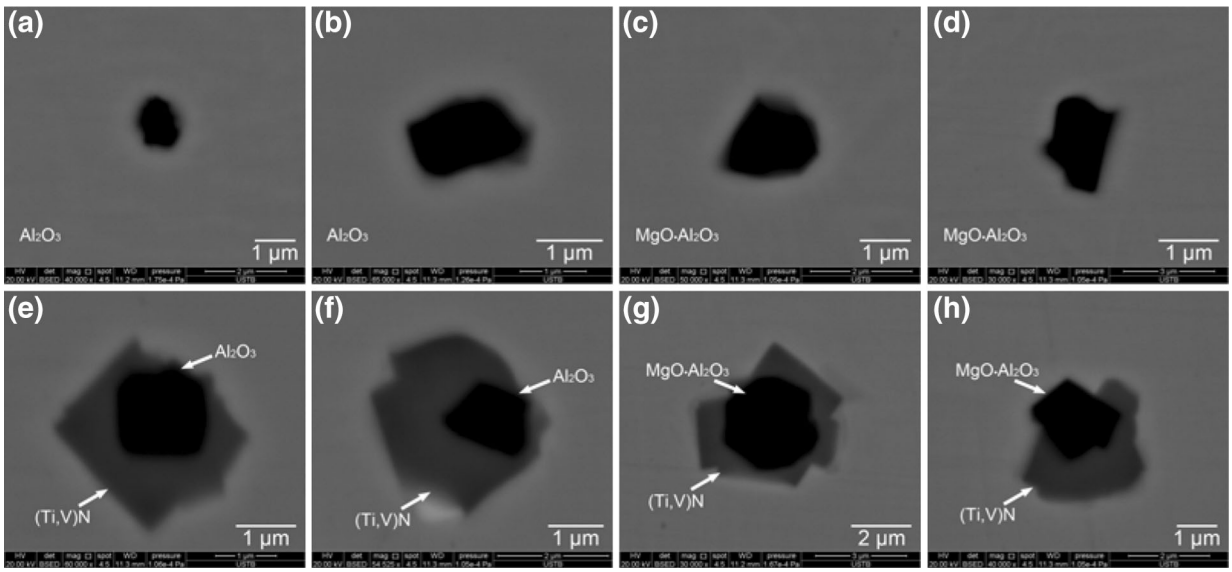

Fig. 3—BSE images and EDS results of typical inclusions observed in ingot ESR-1. (*a*) and (*b*) Al_2O_3, (*c*) and (*d*) $MgO{\cdot}Al_2O_3$, (*e*) and (*f*) dual-phased Al_2O_3 + (Ti,V)N, (*g*) and (*h*) dual-phased $MgO{\cdot}Al_2O_3$ + (Ti,V)N.

$CaO\text{-}MgO\text{-}Al_2O_3$ inclusions are spherical in morphology, which is evidence of their liquid state in liquid steel. In addition, there are many dual-phased precipitates in the form of an Al_2O_3 or $MgO{\cdot}Al_2O_3$ inclusion core fully surrounded by a nitride (Ti,V)N (see Figure 7), and most of these dual-phased precipitates are associated with primary carbides as shown in Figures 7(c) and (e). No pure Al_2O_3 and $MgO{\cdot}Al_2O_3$ inclusions were observed in this ingot.

In the case of remelting with a large calcium addition, the oxide inclusions in remelted ingot were identified as calcium aluminates, whereas no Al_2O_3 and $MgO{\cdot}Al_2O_3$ inclusions were observed. Figure 8 illustrates the SEM micrograph and element mappings of typical inclusions. $CaO\text{-}MgO\text{-}Al_2O_3$ inclusions with homogeneous compositions containing a very small amount of MgO and $CaO\text{-}Al_2O_3$ inclusions with evenly distributed elements are the dominant oxide inclusions in the ingot. Furthermore, still a small proportion of partially modified oxide inclusions by calcium were observed, as shown in Figures 8(c) and 9. An example of a partially extracted inclusion in the ingot is presented in Figure 9. It is clear that MgO and Al_2O_3 concentrated in the core that contains a trace amount of CaO. The concentration of Al_2O_3 decreases outward along the radius of the inclusion. Conversely, CaO concentrated at the outside layer where Al_2O_3 was poor and contained a trace amount of MgO. It suggests that $MgO{\cdot}Al_2O_3$ inclusion is progressively reduced by calcium accompanied by the reaction of calcium with Al_2O_3 in the $MgO{\cdot}Al_2O_3$ inclusion to yield a modified $CaO\text{-}MgO\text{-}Al_2O_3$ inclusion. The MgO content in the modified $CaO\text{-}MgO\text{-}Al_2O_3$ system inclusions is extremely low.

It should be mentioned that, according to SEM–EDS determination, there are no dual-phased inclusions of unreacted $MgO{\cdot}Al_2O_3$ core surrounded by a calcium aluminate layer in calcium-treated ingots, whereas this is the typical type of calcium-modified $MgO{\cdot}Al_2O_3$ inclusions observed by other researchers.[1,15,35,36] A detailed explanation of the difference in the extent of $MgO{\cdot}Al_2O_3$ inclusions modification will be presented later.

A small fraction of CaS inclusions was present in calcium-treated ingots. It is of interest to note that all CaS inclusions are invariably associated with modified calcium aluminate inclusions, as shown in Figures 5(b) and (d), 8(c) and (d). In most cases, CaS exhibits as a thin ring surrounding calcium aluminate inclusions. This observation differs with the finding in calcium treatment of spinels in ESR of ultralow-sulfur steel.[28]

No modified calcium aluminate inclusions (not only the fully but also the partially modified) with associated nitrides or primary carbides were found in calcium-treated ingots. It suggests that modification of alumina and $MgO{\cdot}Al_2O_3$ inclusions to calcium aluminates could prevent the formation of nitrides and primary carbides that have preferred nucleation sites, arising from the elimination of heterogeneous nucleation sites.

3. *Composition distribution of inclusions in remelted ingots*

Modifying oxide inclusions to a lower melting temperature state could improve the deformability of the inclusions.[11–16] This is the aim of oxide inclusions control by refining slag or calcium treatment in many cases.[11–16] The chemistry of the oxide inclusions (excluding CaS in dual-phased $CaO\text{-}Al_2O_3$-(MgO) + CaS) in calcium-treated ingots was depicted on a ternary $CaO\text{-}MgO\text{-}Al_2O_3$ phase diagram, as shown in Figure 10. The compositions of the oxide inclusions that act as the core for nitride and carbide were also plotted on this phase diagram. The region surrounded by a solid line and a dashed line in this phase diagram is the low-melting-temperature region (solid line <1873 K (1600 °C), dashed line <1773 K (1500 °C)) calculated using FactSage 6.4 with FToxid database (ThermFact/CRCT, Montréal, Canada). The compositions of most $CaO\text{-}MgO\text{-}Al_2O_3$ system inclusions in ESR-2 were observed to locate in the liquid region or close to it, as presented in Figure 10(a). However, many modified oxide inclusions still fall out of the liquid region at 1873 K (1600 °C). In the case of a large calcium addition during P-ESR, the compositions of inclusions in the remelted ingot lie in or nearby the low-melting-temperature region (see Figure 10(b)), indicating that the plasticization of oxide inclusions was improved.

4. *Transient inclusions in liquid metal pool during P-ESR refining*

To reveal the inclusion evolution and modification by calcium, the liquid steel samples collected from a liquid metal pool during P-ESR were determined by SEM–EDS. The SEM–EDS results are shown in Figures 11 through 14. It should be pointed out that no sulfide inclusions (not only calcium sulfide but also manganese sulfide) were present in these steel samples.

In the case of no calcium treatment, the inclusions are Al_2O_3 and $MgO{\cdot}Al_2O_3$ in the liquid metal pool. The typical inclusions are shown in Figure 11. It could be noted that the types of inclusions were not changed during ESR without calcium treatment until in ESR ingot.

Figures 12 and 13 show examples of inclusions in the sample collected from the liquid metal pool during P-ESR T2. The inclusions are mainly partially modified inclusions consisting of a $CaO\text{-}MgO\text{-}Al_2O_3$ core surrounded by an outer $CaO\text{-}Al_2O_3$ layer, as evidenced by the element mappings (see Figure 12(a)). MgO was enriched in the core, whereas CaO concentrated in the outside layer of the inclusion. Al_2O_3 distributes evenly throughout the cross section of the inclusion. In addition, $CaO\text{-}MgO\text{-}Al_2O_3$ and $CaO\text{-}Al_2O_3$ inclusions with uniform elements distribution were also found; an example is shown in Figure 12(b). In addition, many alumina and $MgO{\cdot}Al_2O_3$ inclusions were found as shown in Figures 13(a) and (b).

Figure 14 shows the element mappings of typical inclusions observed in the sample collected from the liquid metal pool during P-ESR T3. The dominant inclusions are $CaO\text{-}MgO\text{-}Al_2O_3$ and $CaO\text{-}Al_2O_3$, both of which are homogeneous in compositions. In addition, a small amount of dual-phased $CaO\text{-}MgO\text{-}Al_2O_3$ + $CaO\text{-}Al_2O_3$ inclusions were observed in the sample. Some of these dual-phased inclusions were featured with a much lower or higher CaO concentration in the core. The enrichment of MgO in the core of modified $CaO\text{-}MgO\text{-}Al_2O_3$ inclusions could be clearly observed, as can be seen in Figures 14(b) and (c). In some cases, the concentration of CaO is higher, whereas Al_2O_3 is lower in the region of MgO-free or with a trace amount of MgO (outside layer of the inclusion), compared with that in the core of the inclusion as shown in Figure 14(b). No alumina and $MgO{\cdot}Al_2O_3$ inclusions were found in the liquid metal pool in this heat.

C. *Transient Evolution of Sulfide Inclusions in P-ESR Process*

It was confirmed by SEM–EDS determination that there were no manganese sulfide inclusions found in the liquid metal pool for each heat and in each ESR ingot, indicating that all original manganese sulfide inclusions have been removed before liquid metal droplets collect in the liquid metal pool during P-ESR. The chemical reaction for manganese sulfide inclusion formation in liquid steel is expressed as[37]:

$$[\mathrm{Mn}] + [\mathrm{S}] = (\mathrm{MnS})\ \Delta G_2^\circ = -168822 + 98.87T(\mathrm{J/mol}) \quad [2]$$

The temperature of liquid metal film at the electrode tip in the ESR process is close to the liquidus temperature of electrode steel,[28,38] and its superheat could hardly exceed 20 K to 30 K (20 °C to 30 °C).[38–40] Thus, the temperature of the liquid metal film in the current ESR refining was taken as the liquidus temperature of 8Cr17MoV steel. The liquidus temperature and solidus temperature of the steel were calculated by Thermo-Calc as 1697 K and 1561 K (1424 °C and 1288 °C), respectively. The Gibbs free energy change for reaction [2] was calculated to be 81.46 kJ/mol at 1697 K (1424 °C), on the basis of the value of ΔG_2°, first-order interaction parameters summarized in Table III, and available second-order interaction parameters as:[41] $r_S^C =$

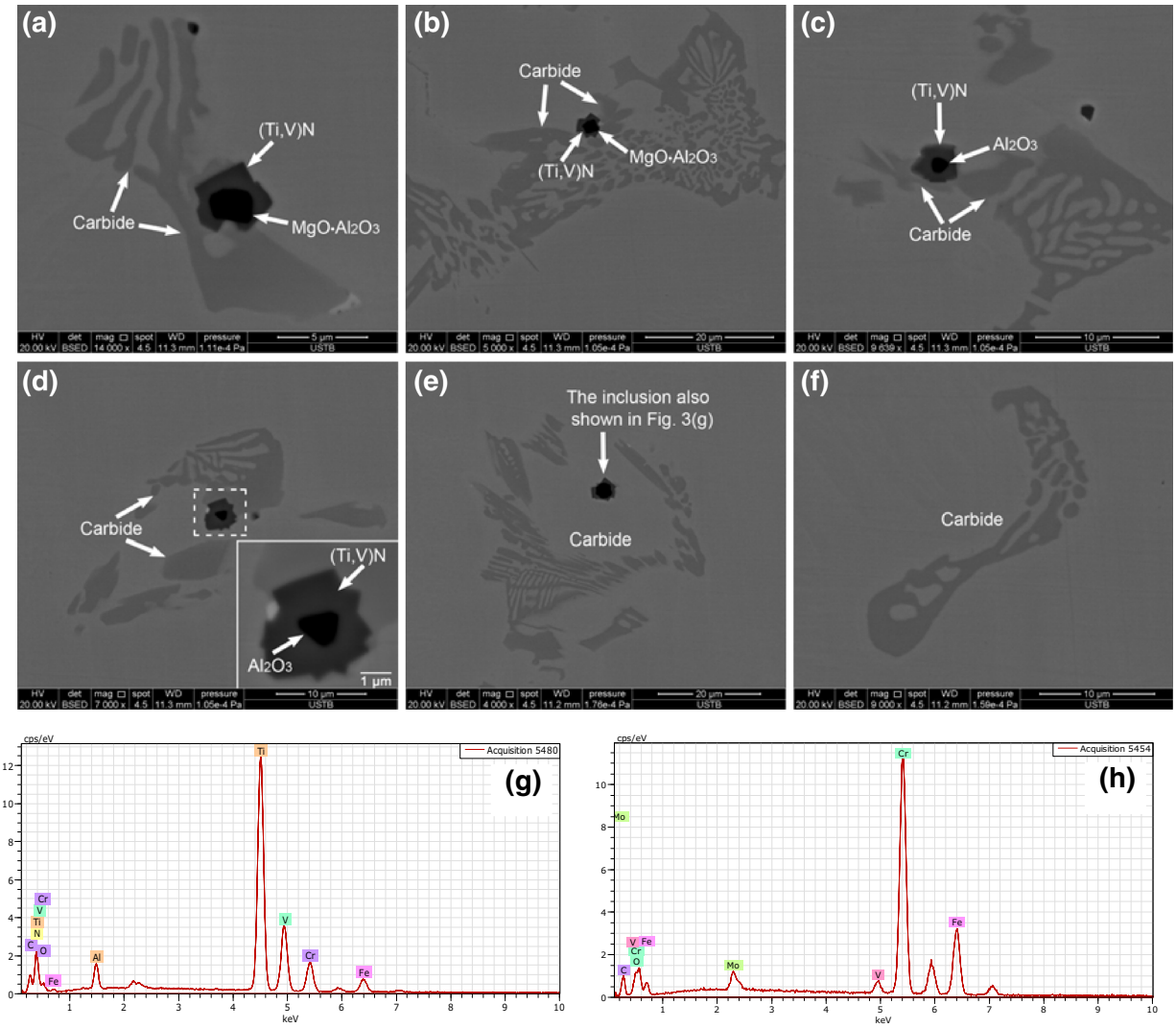

Fig. 4—BSE images and EDS results of primary carbides in as-cast ingot ESR-1. (EDS spectrums shown in (*g*) and (*h*) correspond to the nitride and carbide shown in (*a*) and (*f*), respectively.).

0.0058, $r_S^{Si} = 0.0017$, $r_S^S = -0.0009$, $r_S^{Al} = 0.0009$. This extremely positive Gibbs free energy change indicated that reaction [2] took place toward the left-hand side. Thus, it was concluded that the dissociation of MnS inclusions into dissolved sulfur and manganese in liquid steel occurred during liquid metal film formation and subsequent collection into droplets at the electrode tip. That is why original manganese sulfide inclusions have been completely removed during the P-ESR process.

The aforementioned experimental results showed that calcium sulfide inclusions did not precipitate in the liquid metal pool, whereas they presented as a thin ring surrounding modified calcium aluminate inclusion in as-cast ingot. The starting precipitation temperatures of CaS inclusions in the P-ESR heat T2 and T3 were calculated to be 1495 K (1222 °C) and 1524 K (1251 °C), respectively, by using the thermodynamic data of standard Gibbs free energy change ($\Delta G^\circ = -530{,}900 + 116.2T$[34] (J/mol)) of reaction [Ca] + [S] = (CaS), first-order interaction parameters listed in Table III, and available second-order interaction parameters listed as[42] $r_{Ca}^C = 0.012$, $r_{Ca}^{Si} = 0.0009$, $r_{Ca}^O = 2.6 \times 10^5$, $r_{Ca}^{Al} = 0.0007$. The current thermodynamic analysis indicates that it is in the progress of liquid steel solidification that calcium sulfide inclusions precipitate.

As the temperature of liquid steel drops from liquid metal pool bulk to the bottom of the liquid metal pool during P-ESR refining, liquid steel starts solidifying with consequent segregation and enrichment of solute concentrations in interdendritic melt due to the solute rejection from the solid to liquid metal phase. With the progress of liquid steel solidification, calcium sulfide inclusions start forming in the last liquid as a result of the supersaturation of dissolved calcium and sulfur. In this process, some modified calcium aluminate inclusions serve as nucleation sites for calcium sulfide formation. This is in agreement with the finding revealed by Wang *et al.*,[16] but it is different from the results showing that CaS formed due to inclusion overmodification by excessive calcium addition[46] or as a transient reaction product.[1,26,27] Calcium sulfide inclusion is

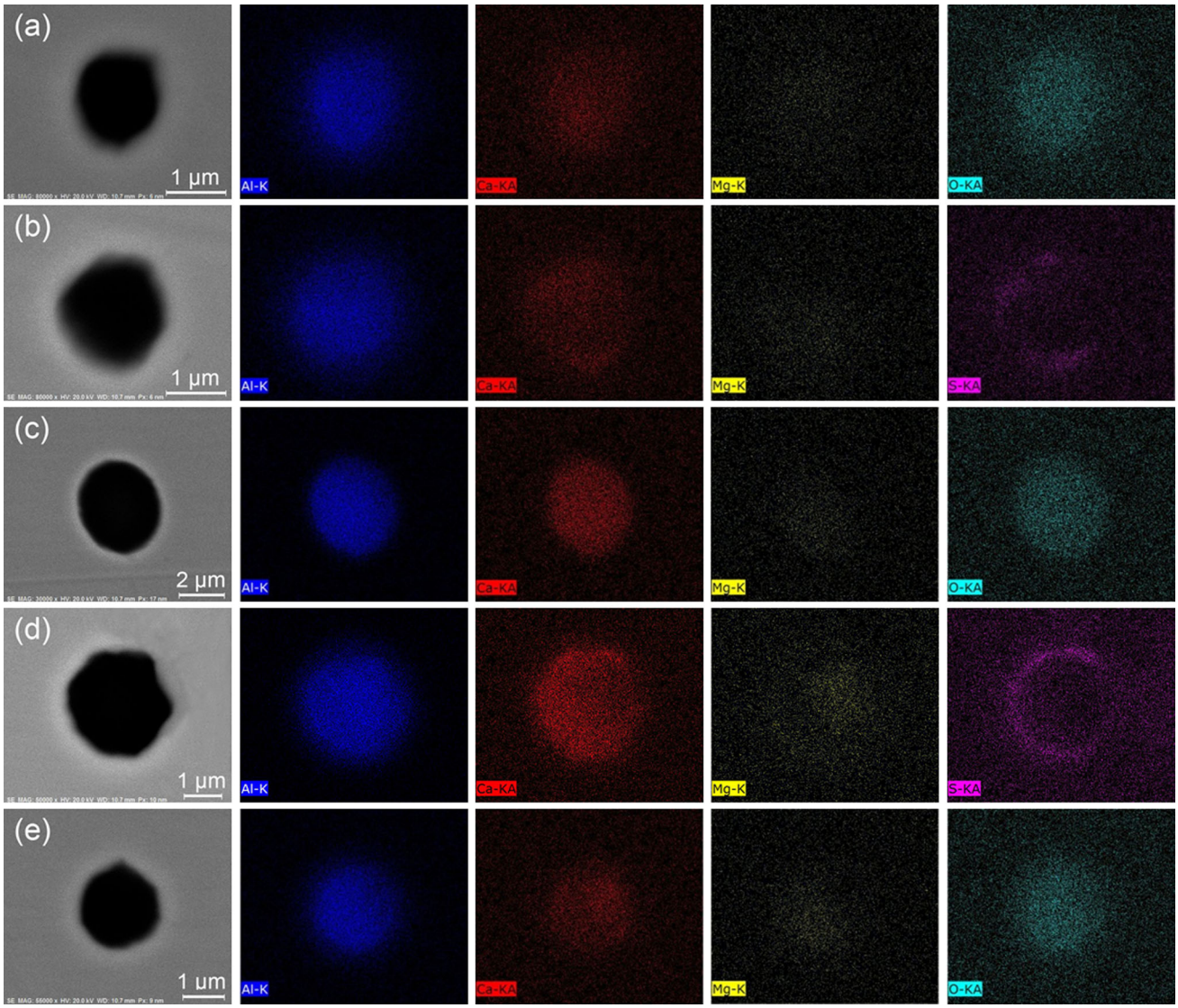

Fig. 5—Element mappings of typical inclusions in ingot ESR-2: (*a*) $CaO\text{-}Al_2O_3$, (*b*) ternary-phased Al_2O_3 + $CaO\text{-}Al_2O_3$ + CaS, (*c*) $CaO\text{-}MgO\text{-}Al_2O_3$, (*d*) ternary-phased $CaO\text{-}MgO\text{-}Al_2O_3$ + $CaO\text{-}Al_2O_3$ + CaS, and (*e*) dual-phased $CaO\text{-}MgO\text{-}Al_2O_3$ + $CaO\text{-}Al_2O_3$ inclusion with a complementary concentration of Ca and Al in Mg-free portion as compared to Mg-enriched portion.

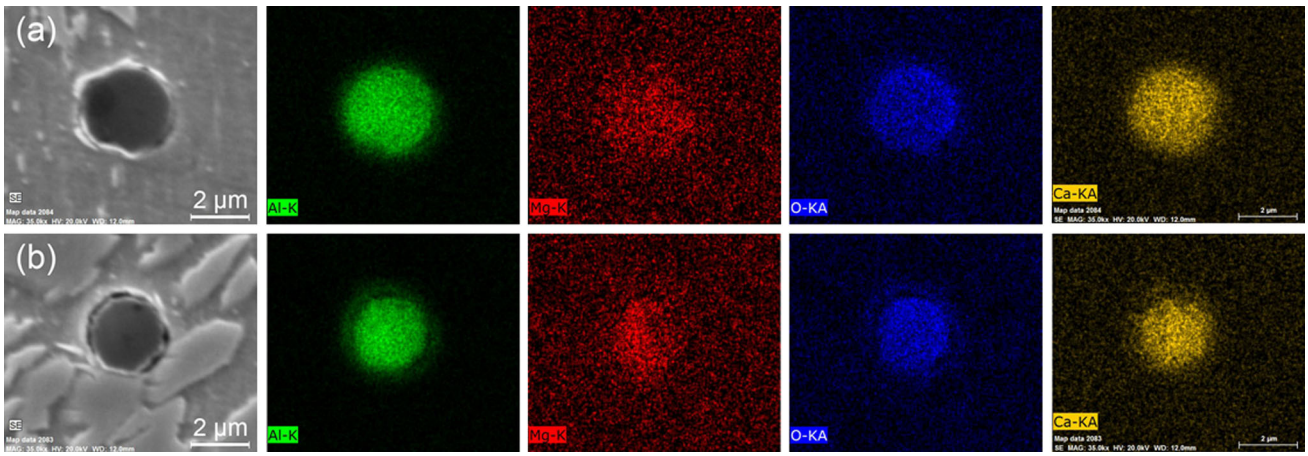

Fig. 6—Element mappings of partially extracted inclusions in ingot ESR-2: (*a*) homogeneous $CaO\text{-}MgO\text{-}Al_2O_3$ inclusion and (*b*) $CaO\text{-}MgO\text{-}Al_2O_3$ inclusion with a complementary concentration of Ca and Mg.

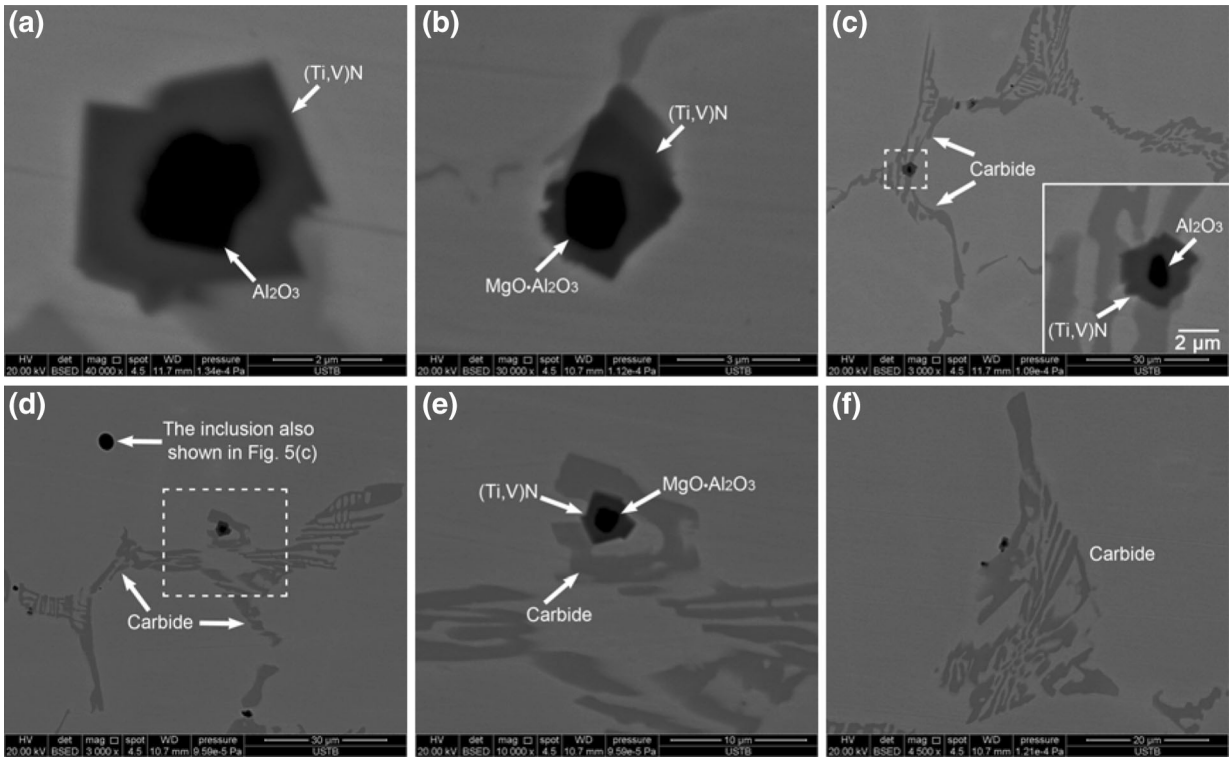

Fig. 7—BSE images and EDS results of multiphase precipitates in as-cast ingot ESR-2. Note: (*e*) is enlarged image of the enclosed area in (*d*).

hardly deformable during rolling.[47] Efforts should always be made to avoid the presence of calcium sulfide inclusions for deep rolling tool steel. One available countermeasure is to reduce the sulfur content of steel to a lower level before achieving calcium modification reaction.

D. *Proposed Mechanism for Modification of Inclusions by Calcium During the P-ESR Process*

In aluminum-killed steel, the dissolved oxygen in liquid steel is determined by both dissolved aluminum in liquid steel and alumina, as expressed by the following equation:[48]

$$\begin{aligned} &2[\mathrm{Al}] + 3[\mathrm{O}] = (\mathrm{Al_2O_3}) \\ &\Delta G_3^{\mathrm{o}} = -1205115 + 386.714T(\mathrm{J/mol}) \end{aligned} \qquad [3]$$

$$K = \frac{a_{\mathrm{Al_2O_3}}}{a_{\mathrm{Al}}^2 \cdot a_{\mathrm{O}}^3} = \frac{a_{\mathrm{Al_2O_3}}}{(f_{\mathrm{Al}}[\mathrm{pct\ Al}])^2 \cdot (f_{\mathrm{O}}[\mathrm{pct\ O}])^3} \qquad [4]$$

where $a_{\mathrm{Al_2O_3}}$ is the activity of alumina. f_{Al} and f_{O} are the activity coefficients of dissolved aluminum and oxygen in liquid steel, respectively, and can be expressed by the following formulas:[49]

$$\lg f_i = \sum \left(e_i^j [\mathrm{pct}\ j] + r_i^j [\mathrm{pct}\ j]^2 \right) \qquad [5]$$

where e_i^j and r_i^j are the first-order and second-order interaction parameters, respectively. The first-order interaction parameters used in the present study are listed in Table III. The available second-order interaction parameters are as follows: $r_{\mathrm{Al}}^{\mathrm{C}} = -0.004$,[42] $r_{\mathrm{Al}}^{\mathrm{Si}} = -0.0006$,[42] $r_{\mathrm{Al}}^{\mathrm{Al}} = -0.0011 + 0.17/T$,[42] $r_{\mathrm{O}}^{\mathrm{Ni}} = 0.00011$,[43] $r_{\mathrm{O}}^{\mathrm{Cr}} = 0.00058$,[4] $r_{\mathrm{O}}^{\mathrm{Al}} = 0.0033 - 25/T$.[50]

The activity of Al_2O_3 in the CaF_2-containing ESR slag was calculated using FactSage 6.4 (CON2 database) as 0.015 at 1873 K (1600 °C). This database includes all thermodynamic data for component CaF_2 in molten slag. The dissolved oxygen in equilibrium with Al_2O_3 was calculated to be 2 ppm in the liquid metal pool. The measured total oxygen content is 40 ppm in remelted ingot. The total oxygen in steel includes both the dissolved oxygen (free oxygen) and the oxygen bonded as oxide inclusions. Thus, this extremely low dissolved oxygen would contribute inconsiderably to the generation of newly formed oxide inclusions in the liquid metal pool during solidification of liquid steel, as well as to the proportion of total oxide inclusions.

The aforementioned analysis demonstrated that all calcium sulfide inclusions observed in as-cast ingot were that formed at the bottom of the liquid metal pool during liquid steel solidification, and they nucleated on CaO-Al_2O_3-(MgO) inclusions rather than in liquid steel (as discussed earlier). Even though formation of metastable CaS inclusions cannot be completely excluded due to a high local concentration of calcium in liquid steel after calcium injection, calcium sulfide is not transient inclusion during the current P-ESR refining as demonstrated by SEM observations of the samples taken from the liquid metal pool. Consequently, it was considered that calcium sulfide did not take part in the modification of alumina and $MgO{\cdot}Al_2O_3$

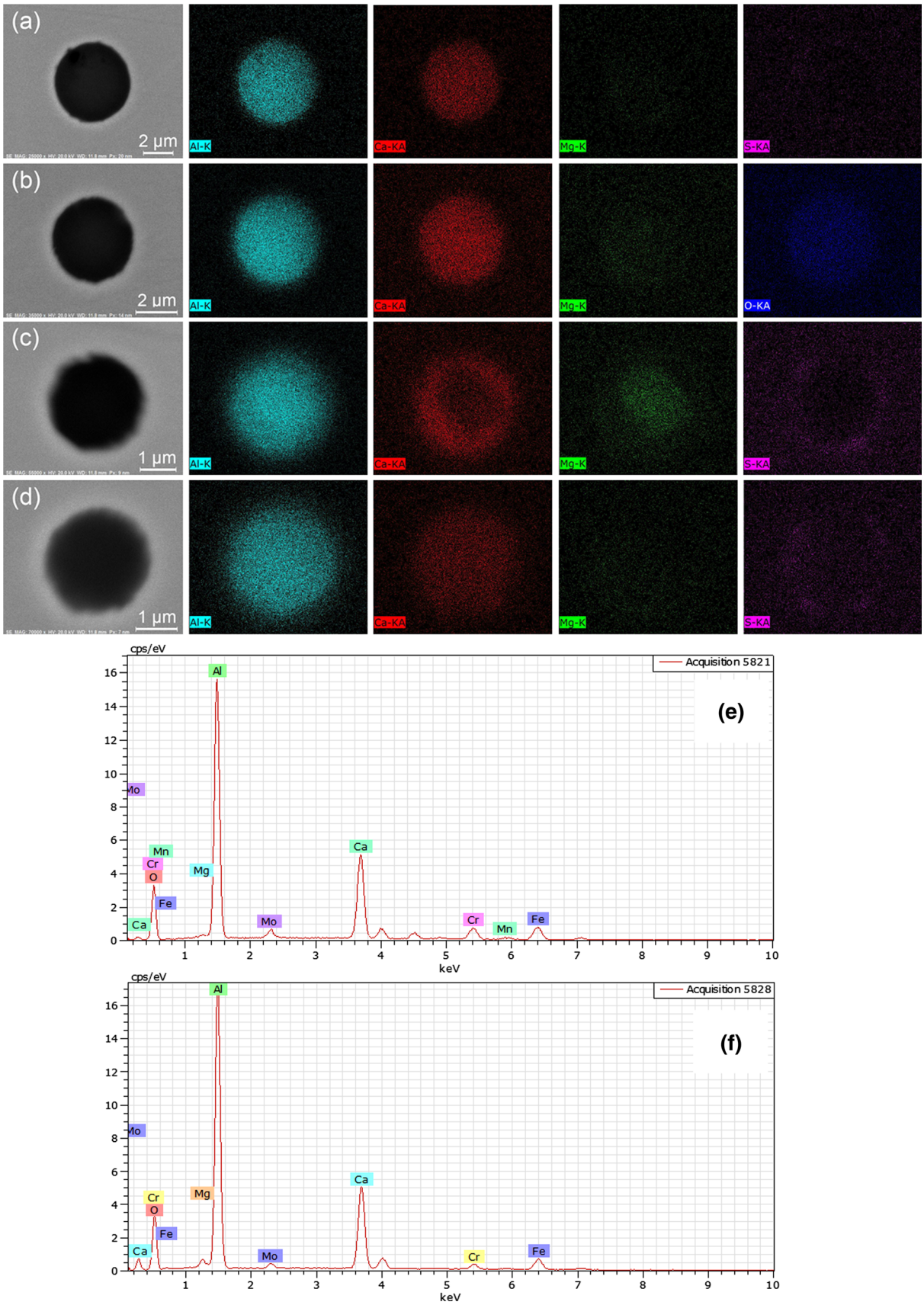

Fig. 8—Element mappings of typical inclusions observed in ingot ESR-3. (*a*) CaO-Al_2O_3, (*b*) CaO-MgO-Al_2O_3, (*c*) ternary-phased CaO-MgO-Al_2O_3 + CaO-Al_2O_3 + CaS, and (*d*) dual-phased CaO-Al_2O_3 + CaS. (EDS spectrums shown in (*e*) and (*f*) correspond to the oxide inclusions shown in (*a*) and (*b*), respectively.).

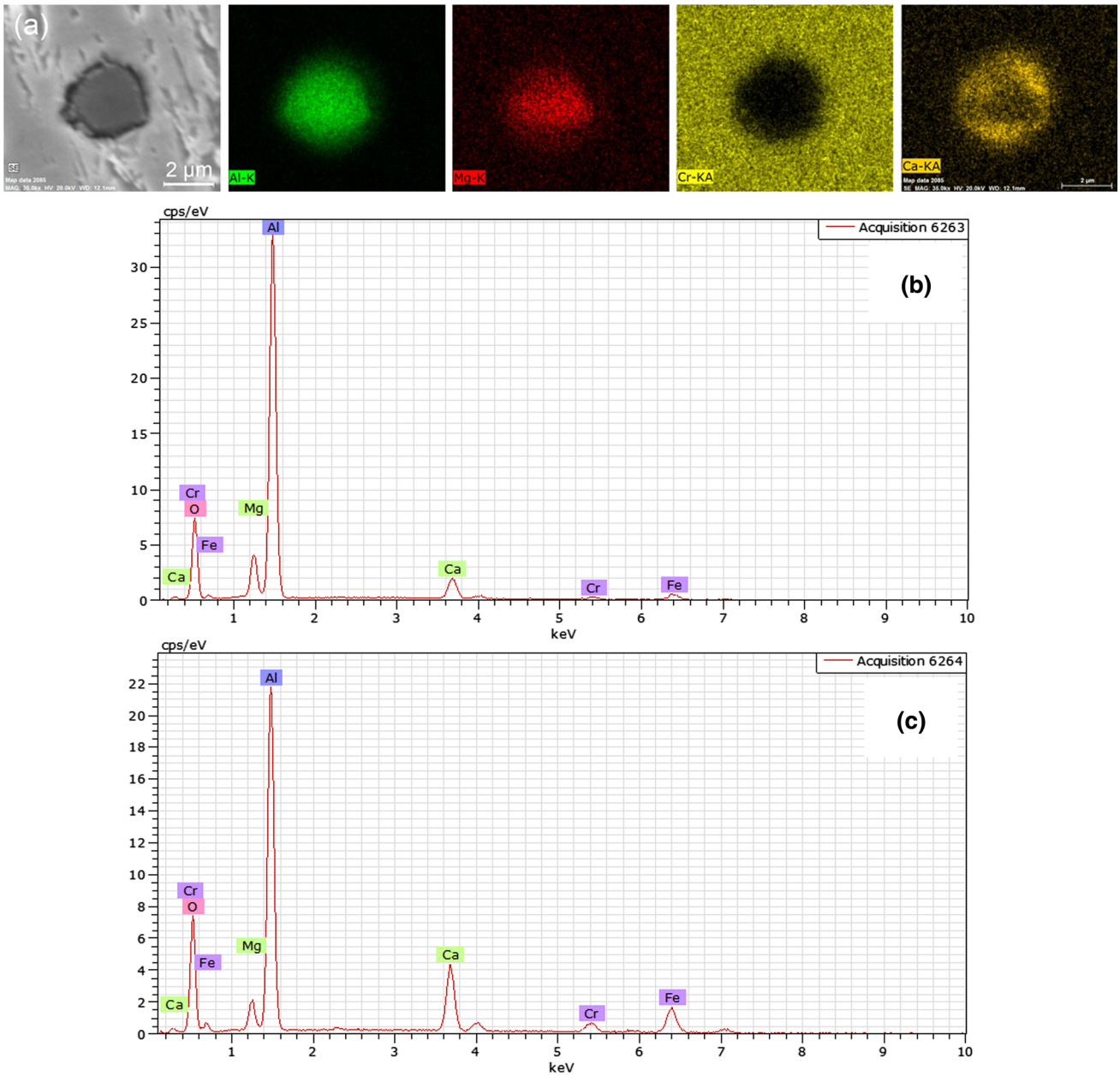

Fig. 9—Element mappings of a partially extracted inclusion in as-cast ingot ESR-3. (MgO and Al_2O_3 are enriched in the core and poor at the outside layer; CaO showed opposite distribution.) Note: (*b*) and (*c*) present the point analysis EDS spectrums, which correspond to the center and the edge of the inclusion shown in (*a*), respectively.

inclusions by calcium. This result agrees well with that showing an absent role of calcium sulfide in calcium modification of alumina or $MgO{\cdot}Al_2O_3$ inclusions reported in previous studies.[17–25,35,36] But the current finding is different from the observations reported by Verma *et al.*[1,26,27] who showed that CaS formed adhering to alumina or spinel immediately after calcium injection (through sampling the steel melt 2 and 4 minutes after calcium injection, together with subsequent SEM determination), and subsequently reacted with Al_2O_3 contained in the inclusions resulting in the modification of alumina and spinel inclusions.

From experimental determination of transient inclusions and the inclusions in as-cast ingots, the results showed that the original alumina and $MgO{\cdot}Al_2O_3$ inclusions (except for that had been removed during P-ESR) were fully modified to mainly CaO-MgO-Al_2O_3 or CaO-Al_2O_3 inclusions with homogeneous compositions by calcium treatment. Partially modified inclusions (consisting of a CaO-MgO-Al_2O_3 core surrounded by a liquid CaO-Al_2O_3 layer) also account for a small proportion not only in liquid metal pool but also in as-cast ingot. In the case where there is a small calcium addition, unmodified alumina and $MgO{\cdot}Al_2O_3$ inclusions indeed remain in the whole P-ESR process until in remelted ingot.

Partially modified inclusions of an unreacted alumina or CaO-MgO-Al_2O_3 core surrounded by an outer

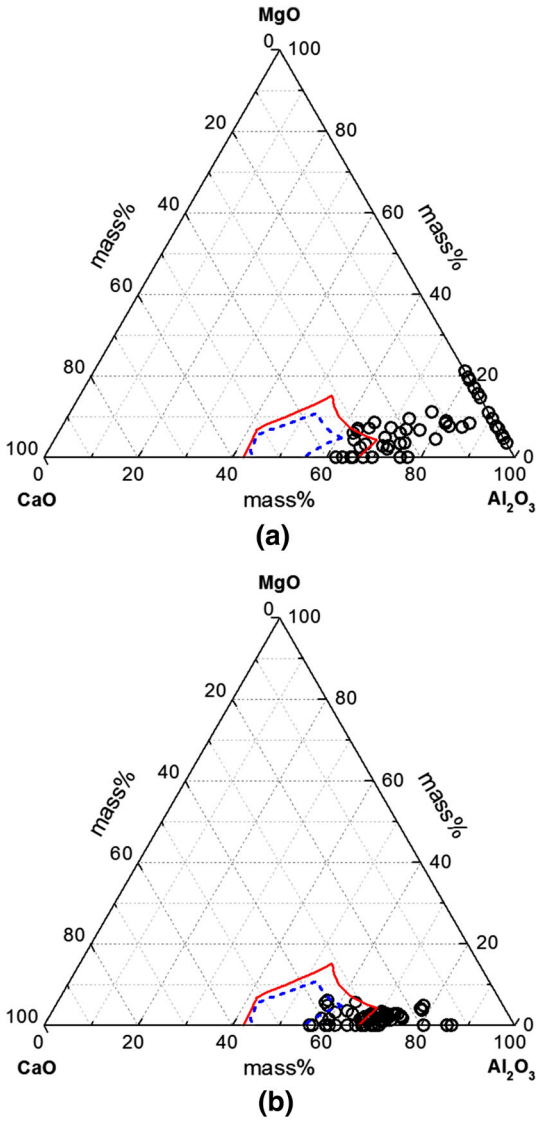

Fig. 10—Composition distribution of oxide inclusions in remelted ingots on ternary CaO-MgO-Al_2O_3 diagram: (*a*) ESR-2 and (*b*) ESR-3 [dashed line <1773 K (1500 °C) and solid line <1873 K (1600 °C)].

CaO-Al_2O_3 layer provided an indication that the original alumina and MgO·Al_2O_3 inclusions were gradually modified by dissolved calcium from outside to inside. The observations revealed that the MgO content was reduced in the calcium-modified inclusions (compared with original oxide inclusions, and those partially modified CaO-MgO-Al_2O_3 system inclusions). This is more intuitively in partially modified CaO-MgO-Al_2O_3 inclusions (comparing the core with the outside layer of the inclusion, two examples are shown in Figures 5(d) and 8(c)).

It is considered that the modification of spinel inclusions progresses through reducing magnesium oxide progressively from the spinel by calcium from outside to inside. This reaction generates the fully modified CaO-Al_2O_3 inclusions with evenly distributed components, and incomplete transformation of MgO·Al_2O_3 to CaO-MgO-Al_2O_3 inclusions with homogeneous compositions or dual-phased inclusions of an outer CaO-Al_2O_3 layer forming around the CaO-MgO-Al_2O_3 core. The reactions involved in the modification are as follows:

$$[\mathrm{Ca}] + \mathrm{MgO}\cdot x\mathrm{Al_2O_3(s)} = \mathrm{CaO}\cdot x\mathrm{Al_2O_3(s)} + [\mathrm{Mg}] \quad [6]$$

$$[\mathrm{Ca}] + x\mathrm{MgO}\cdot y\mathrm{Al_2O_3(s)} = \mathrm{CaO}\cdot(x-1)\mathrm{MgO}\cdot y\mathrm{Al_2O_3(s)} + [\mathrm{Mg}] \quad [7]$$

The mechanism presented here for spinels modification is basically consistent with that proposed by Pretorius *et al.*[20] in modifying MgO·Al_2O_3 spinels in LACK steel by calcium, but apparently it is different from that suggested by Verma *et al.*[1,30] and Yang *et al.*[35]

In the modification of low-MgO-containing MgO·Al_2O_3 inclusions, not only Mg but also Al was reduced from the original inclusion (see examples in Figures 5(e), 9, and 14(b)). This modification involves both the preferential reduction of MgO from the MgO·Al_2O_3 inclusion by calcium and the reaction of calcium with Al_2O_3 in the inclusion. This route is significantly different from that of spinels modification revealed not only in the current study but also by other researchers.[1,20,30,35]

For modification of alumina inclusions by calcium, injected calcium reacts with alumina directly, thereby forming CaO-Al_2O_3 inclusions with uniformly distributed elements or incompletely modified dual-phased inclusions of an unreacted alumina core surrounded by an outer CaO-Al_2O_3 layer, as represented by the following reaction:

$$[\mathrm{Ca}] + (x+1/3)\mathrm{Al_2O_3(s)} = \mathrm{CaO}\cdot x\mathrm{Al_2O_3(s)} + 2/3[\mathrm{Al}] \quad [8]$$

The calcium modification reaction of these inclusions could be assumed to progress in the form of an unreacted core model, as suggested by Park *et al.* in calcium modification of alumina inclusions[25] and aluminum modification of MgO to MgO·Al_2O_3 inclusion.[51] In the process of calcium treatment, calcium element diffused into the inner part of the inclusion through newly formed calcium aluminates layer gradually, and the formed product elements diffused in an opposite way. The transformation reaction occurred at the newly formed intermediate layer/unreacted inclusion core interface.

Except for those having been removed in the P-ESR process, all original alumina were completely modified to homogenous CaO-Al_2O_3 inclusions, but insufficient modification of MgO·Al_2O_3 remained (occupying a small proportion). Despite the insufficient modification, however, there are no unreacted MgO·Al_2O_3 or Al_2O_3 cores in the partially modified inclusions. The current result is different from the observations reported by other researchers.[1,15,35,36] These findings indicate that the inclusion modification in the ESR process is more thorough than that in other refining practices. The

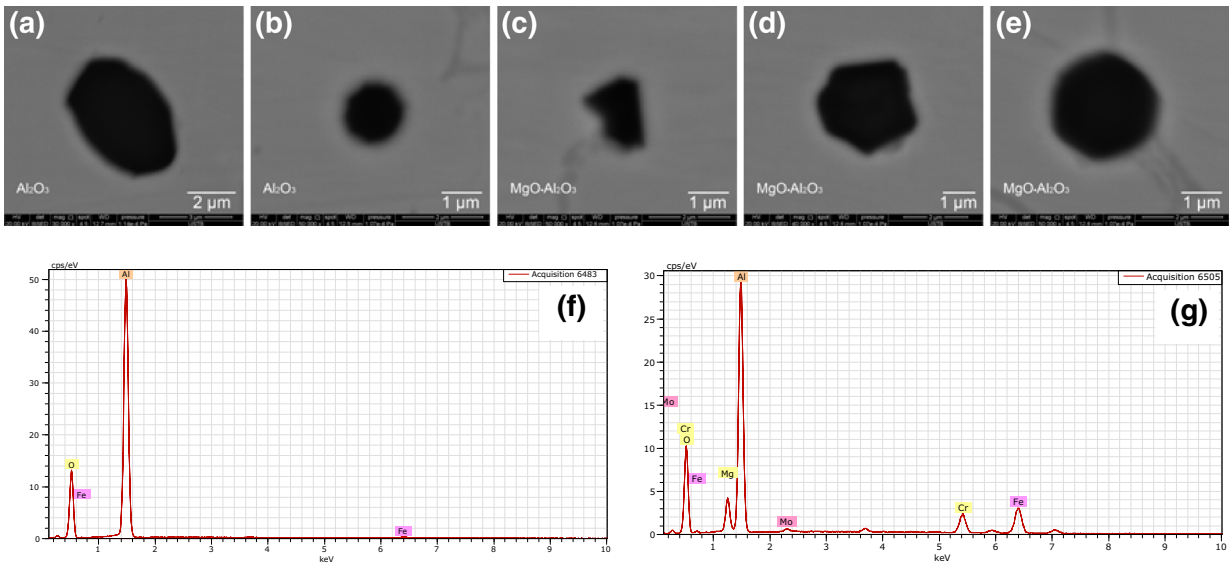

Fig. 11—Typical inclusions observed in the sample collected from the liquid metal pool during ESR T1. (EDS spectrums shown in (*f*) and (*g*) correspond to the oxide inclusions shown in (*a*) and (*e*), respectively.).

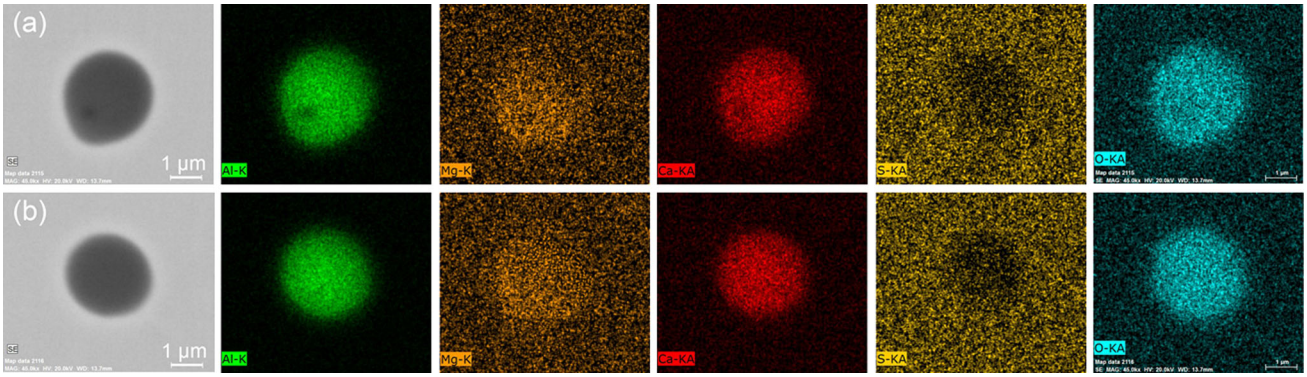

Fig. 12—Element mappings of typical inclusions in the sample sampled from the liquid metal pool during ESR T2: (*a*) a dual-phased CaO-MgO-Al_2O_3 + CaO-Al_2O_3 and (*b*) a homogeneous CaO-MgO-Al_2O_3 inclusion.

inclusion modification is determined not only by thermodynamic but also by kinetic constraints. The superior inclusion modification is expected to be attributed to preferable conditions (namely, small size of original inclusions (mostly 1 to 4 μm), long chemical reaction time, and high ratio of surface o volume between the liquid metal film at the electrode tip and slag[52,53]) in ESR refining, which are beneficial to the reaction kinetics of calcium modification.

The previous research[4,36,54] demonstrated that even at a few ppm of dissolved calcium, calcium aluminates could form from alumina and spinel inclusions, whereas excessive calcium addition led to CaS formation in liquid steel, which was indicative of overmodification of inclusions by calcium.[46] The current study confirmed that the formation of CaS inclusion initiated in the progress of liquid steel solidification, and the formed CaS adhered to calcium aluminates (even though incompletely modified). Thus, the formation of CaS cannot be exclusively attributed to excessive calcium addition. Further study should be made to establish chemical composition conditions for achieving full liquefaction of oxide inclusions with favorable deformability but without forming CaS. To this end, it was suggested from the current results that the sulfur content, rather than calcium, of liquid steel should be reduced to a lower level. It is realizable in ESR refining, as demonstrated in previous ESR practice.[28]

The total oxygen and magnesium contents of stainless steel were not further reduced even when calcium addition was employed in the P-ESR refining, which was an evidence of the absent contribution of calcium to oxide inclusions removal. It is attributed to the fact that the modified low-melting-point calcium aluminate inclusions are removed less easily and thoroughly from liquid steel than solid inclusions (alumina and spinel) because of their smaller contact angle.[55–58] Similar observations were also reported by Yang *et al.*[55] and Reis *et al.*[58] through laboratory crucible experiments and industrial secondary refining practice.

The remelted ingots confirmed that all alumina and MgO·Al_2O_3 inclusions that had not been removed in the

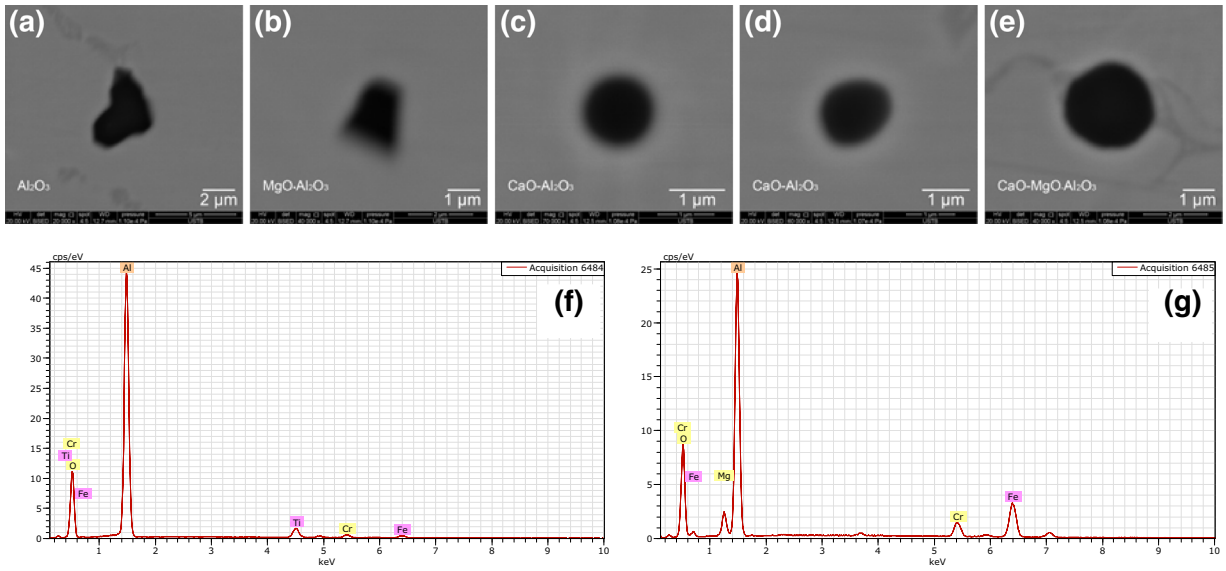

Fig. 13—Typical inclusions in the sample sampled from the liquid metal pool during ESR T2. (EDS spectrums shown in (*f*) and (*g*) correspond to the oxide inclusions shown in (*a*) and (*b*), respectively.).

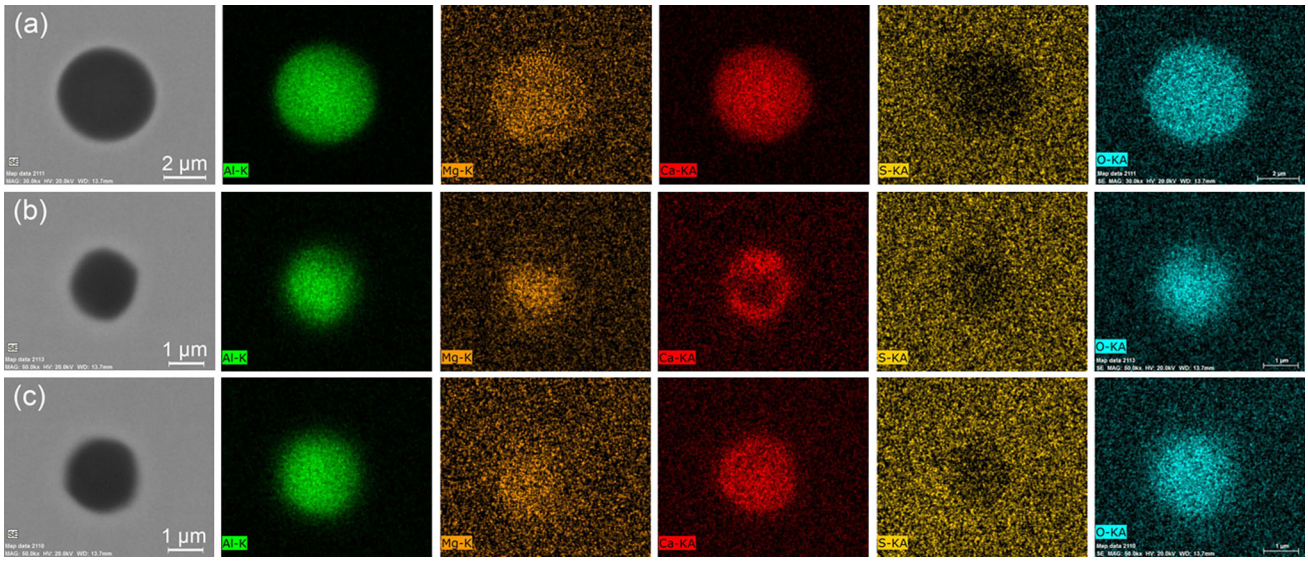

Fig. 14—Element mappings of typical inclusions in the sample collected from the liquid metal pool during ESR T3: (*a*) CaO-MgO-Al_2O_3 inclusion and (*b*) and (*c*) dual-phased CaO-MgO-Al_2O_3 + CaO-Al_2O_3 inclusion with lower or higher CaO concentration in the core, respectively. Note: The inclusion in (b) is featured with a complementary concentration of Ca and Al at the outside layer.

Table III. First-Order Interaction Parameters e_i^j Used in the Present Study

i (j→)	C	Si	Mn	S	Ni	Cr	V	Mo	Ca	O	Al
Mn	−0.0538	−0.0327	0	−0.048	−0.0072	0.0039	0.0057	0.0046	—	−0.083	—
S	0.111	0.075	−0.026	−0.046	0	0.0105	−0.019	0.0027	−110	−0.27	0.041
Ca	−0.34	−0.096	−0.0156[42]	−140	−0.044	0.014[43]	—	—	−0.002	−2500[42]	−0.072
O	−0.421	−0.066	−0.021	−0.133	0.006	−0.033[4]	−0.14	0.005	—	−0.17	−1.17
Al	0.091	0.056	0.035[44]	0.035	−0.029[4]	0.0096[4]	—	—	−0.047[4]	−1.98[4]	0.045[4]

Note: The data without notation are from Ref. [45].

P-ESR process served as preferred nucleation sites for promoting nitrides and primary carbides formation, whereas it is not the case for calcium aluminate inclusions (not only the fully but also the partially modified). It is suggested that calcium modification of oxide inclusions during ESR refining could indirectly

control nitrides and primary carbides formation. Similarly, heterogeneous nucleation of TiN on alumina inclusion was reported by Suito *et al.*,[59] and on $MgO{\cdot}Al_2O_3$ spinel was observed by Park *et al.*;[60,61] a crystallographic relationship between TiN and oxide inclusions in view of the planar lattice disregistry concept was presented in their studies.[59–61] If only targeting the restraint of nitrides and primary carbides formation, it is indeed not indispensable to achieve full liquefaction of oxide inclusions, as demonstrated by the current results. Further discussion on the nucleation potency among oxide inclusions, nitrides, and primary carbides in ESR refining will be presented in the next article of the present series,[62] as well as in the phase characterization of these primary carbides.

IV. CONCLUSIONS

The modification of alumina and $MgO{\cdot}Al_2O_3$ inclusions by calcium treatment during P-ESR of 8Cr17MoV stainless steel containing high sulfur and oxygen was investigated. This study was also conducted to reveal the effect of oxide inclusions modification on nitrides and primary carbides in as-cast ingot. The following conclusions were drawn:

1. Calcium treatment made no contribution to further reducing oxygen and sulfur contents, as well as increasing oxide inclusions removal during P-ESR refining. The original oxide inclusions in the electrode were Al_2O_3 and $MgO{\cdot}Al_2O_3$, among which had not been removed during P-ESR remained until in as-cast ingots.
2. Except for those having been removed, calcium treatment during the P-ESR process modified all alumina to liquid/partially $CaO\text{-}Al_2O_3$ inclusions with homogeneous compositions, as well as modified $MgO{\cdot}Al_2O_3$ inclusions to mainly $CaO\text{-}MgO\text{-}Al_2O_3$ or $CaO\text{-}Al_2O_3$ inclusions with evenly distributed elements, together with a small amount of partially modified $CaO\text{-}MgO\text{-}Al_2O_3$ core surrounded by an outer $CaO\text{-}Al_2O_3$ layer.
3. The modification of spinels progresses through preferential reduction of MgO from the spinel by calcium, just like in the case of spinel modification in ultralow-sulfur steel. The modification of low-MgO $MgO{\cdot}Al_2O_3$ inclusions is attributed to the preferential reduction of MgO from the inclusion by calcium accompanied with the reaction of calcium with Al_2O_3 in the inclusion. It is the direct reaction of calcium with alumina that contributes to the full modification of alumina inclusions.
4. Calcium sulfide did not play a role in the modification of alumina and $MgO{\cdot}Al_2O_3$ inclusions by calcium during P-ESR refining, whereas calcium sulfide inclusions were invariably associated with modified calcium aluminate inclusions in as-cast ingots. To achieve the target of full modification of oxide inclusions and prevent the formation of calcium sulfide, the sulfur content, rather than calcium, of liquid steel should be reduced to a lower level.
5. Unlike what all alumina and $MgO{\cdot}Al_2O_3$ inclusions did, the modified calcium aluminate inclusions (both the fully and the partially modified) did not serve as preferred nucleation sites for promoting nitrides and primary carbides formation. All observed nitrides (Ti,V)N possessed an alumina or $MgO{\cdot}Al_2O_3$ inclusion as their nucleation site, and almost all these nitrides are associated with the favorable formation of primary carbides.
6. If exclusively targeting the restraint of nitrides and primary carbides formation, it is indeed not indispensable to achieve full liquefaction of oxide inclusions.

ACKNOWLEDGMENTS

The author (C.B. SHI) is grateful to Professor Jung-wook Cho, Pohang University of Science and Technology, for his fruitful discussions. Thanks are also extended to Senior Researcher Guangqi Lv and all other personnel of Zhejiang Zhengda Mould Corp., LTD, for their scientific input in the experimental operations. The financial support by the National Natural Science Foundation of China (Grant Nos. 51504019 and 51444004) and China Postdoctoral Science Foundation (2016T90035) is also greatly acknowledged.

REFERENCES

1. N. Verma, P.C. Pistorius, R.J. Fruehan, M.S. Potter, H.G. Oltmann, and E.B. Pretorius: *Metall. Mater. Trans. B*, 2012, vol. 43B, pp. 830–40.
2. M. Jiang, X.H. Wang, and J.J. Pak: *Metall. Mater. Trans. B*, 2014, vol. 45B, pp. 1248–59.
3. D. Yao, J. Li, J. Li, and Q. Zhu: *Mater. Manuf. Process.*, 2015, vol. 30, pp. 111–15.
4. J.H. Park and H. Todoroki: *ISIJ Int.*, 2010, vol. 50, pp. 1333–46.
5. H.V. Atkinson and G. Shi: *Prog. Mater. Sci.*, 2003, vol. 48, pp. 457–520.
6. K. Fukaura, Y. Yokoyama, D. Yokoi, N. Tsujii, and K. Ono: *Metall. Mater. Trans. A*, 2004, vol. 35A, pp. 1289–1300.
7. M.K. El-Fawkhry, A.M. Fathy, and M.M. Eissa: *Steel Res. Int.*, 2014, vol. 85, pp. 885–90.
8. J. Li, J. Li, C.B. Shi, L.L. Wang, Z. Wu, and H. Wang: *Can. Metall. Q*, 2016, vol. 55, pp. 321–27.
9. P.N. Quested and M. Mclean: *Mater. Sci. Eng.*, 1984, vol. 65, pp. 171–80.
10. K.S. Cho, S.I. Kim, S.S. Park, W.S. Choi, H.K. Moon, and H. Kwon: *Metall. Mater. Trans. A*, 2016, vol. 47A, pp. 26–32.
11. J.I. Takamura and S. Mizoguchi: *Proc. 6th Int. Iron Steel Cong.*, ISIJ, Nagoya, Japan, 1990, p. 591.
12. C. Bertrand, J. Molinero, and S. Landa: *Ironmak. Steelmak.*, 2003, vol. 30, pp. 165–69.
13. K. Wang, M. Jiang, X. Wang, Y. Wang, H. Zhao, and Z. Cao: *Metall. Mater. Trans. B*, 2015, vol. 46B, pp. 2198–207.
14. K. Tomioka, K. Ogawa, and H. Matsumoto: *ISIJ Int.*, 1996, vol. 36, pp. S101–04.
15. M. Jiang, X.H. Wang, B. Chen, and W.J. Wang: *ISIJ Int.*, 2010, vol. 50, pp. 95–104.
16. Y. Wang, M. Valdez, and S. Sridhar: *Metall. Mater. Trans. B*, 2002, vol. 33B, pp. 625–32.
17. L. Holappa, M. Hämäläinen, M. Liukkonen, and M. Lind: *Ironmak. Steelmak.*, 2003, vol. 30, pp. 111–15.
18. S.R. Story and R.I. Asfahani: *AISTech 2013 Proc., Vol. II, Association for Iron & Steel Technology*, Pittsburgh, PA, 2013, pp. 1201–13.
19. Y.I. Ito, S. Nara, Y. Kato, and M. Suda: *Tetsu–to–Hagané*, 2007, vol. 93, pp. 355–61.

20. E.B. Pretorius, H.G. Oltmann, and T. Cash: *Iron Steel Technol*., 2010, vol. 7, pp. 31–44.
21. Z. Deng and M. Zhu: *Steel Res. Int*., 2013, vol. 84, pp. 519–25.
22. W. Yang, L. Zhang, X. Wang, Y. Ren, X. Liu, and Q. Shan: *ISIJ Int*., 2013, vol. 53, pp. 1401–10.
23. S. Yang, J. Li, Z. Wang, J. Li, and L. Lin: *Int. J. Miner., Metall. Mater*., 2011, vol. 18, pp. 18–23.
24. M. Lind and L. Holappa: *Metall. Mater. Trans. B*, 2010, vol. 41B, pp. 359–66.
25. J.H. Park, D.S. Kim, and S.B. Lee: *Metall. Mater. Trans. B*, 2005, vol. 36B, pp. 67–73.
26. N. Verma, P.C. Pistorius, R.J. Fruehan, M. Potter, M. Lind, and S. Story: *Metall. Mater. Trans. B*, 2011, vol. 42B, pp. 711–19.
27. N. Verma, P.C. Pistorius, R.J. Fruehan, M. Potter, M. Lind, and S.R. Story: *Metall. Mater. Trans. B*, 2011, vol. 42B, pp. 720–29.
28. C.B. Shi, X.C. Chen, H.J. Guo, Z.J. Zhu, and X. Sun: *Metall. Mater. Trans. B*, 2013, vol. 44B, pp. 378–89.
29. Y.W. Dong, Z.H. Jiang, Y.L. Cao, A. Yu, and D. Hou: *Metall. Mater. Trans. B*, 2014, vol. 45B, pp. 1315–24.
30. N. Verma, M. Lind, P.C. Pistorius, R.J. Fruehan, and M. Potter: *Iron Steel Technol*., 2010, vol. 7, pp. 189–97.
31. B. Hallstedt: *J. Am. Ceram. Soc*., 1992, vol. 75, pp. 1497–507.
32. G.J.W. Kor: *Proc. of 1st Int. Calcium Treatment Symp*., Glasgow, Scotland, 1988, p. 39.
33. C.B. Shi, X.C. Chen, H.J. Guo, Z.J. Zhu, and H. Ren: *Steel Res. Int*., 2012, vol. 83, pp. 472–86.
34. H. Suito and R. Inoue: *ISIJ Int*., 1996, vol. 36, pp. 528–36.
35. S. Yang, Q. Wang, L. Zhang, J. Li, and K. Peaslee: *Metall. Mater. Trans. B*, 2012, vol. 43B, pp. 731–50.
36. Y.J. Kang, F. Li, K. Morita, and D. Sichen: *Steel Res. Int*., 2006, vol. 77, pp. 785–92.
37. H. Doostmohammadi, P.G. Jönsson, J. Komenda, and S. Hagman: *Steel Res. Int*., 2010, vol. 81, pp. 142–49.
38. J.H. Wei and A. Mitchell: *Acta Metall. Sin*., 1984, vol. 20, pp. B261–79.
39. M.E. Fraser and A. Mitchell: *Ironmak. Steelmak*., 1976, vol. 3, pp. 279–87.
40. A. Mitchell, J. Szekely, and J.F. Elliott: *Electroslag Refining*, London, The Iron and Steel Institute, 1973, pp. 3–15.
41. G.K. Sigworth and J.F. Elliott: *Met. Sci*., 1974, vol. 8, pp. 298–310.
42. H. Ohta and H. Suito: *Metall. Mater. Trans. B*, 1996, vol. 27B, pp. 943–53.
43. H. Ohta and H. Suito: *ISIJ Int*., 2003, vol. 43, pp. 1293–300.
44. J.H. Park, S.B. Lee, D.S. Kim, and J.J. Pak: *ISIJ Int*., 2009, vol. 49, pp. 337–42.
45. The Japan Society for the Promotion of Science: *The 19th Committee on Steelmaking: Steelmaking Data Sourcebook*, Gordon and Breach Science Publishers, New York, NY, 1988.
46. J.M.A. Geldenhuis and P.C. Pistorius: *Ironmak. Steelmak*., 2000, vol. 27, pp. 442–49.
47. S.K. Choudhary and A. Ghosh: *ISIJ Int*., 2008, vol. 48, pp. 1552–59.
48. M.A.T. Andersson, P.G. Jönsson, and M.M. Nzotta: *ISIJ Int*., 1999, vol. 39, pp. 1140–49.
49. C.H.P. Lupis: *Chemical Thermodynamics of Materials*, Elsevier Sci. Pub. Co., Inc., New York, 1983, p. 236.
50. H. Itoh, M. Hino, and S. Ban-ya: *Tetsu–to–Hagané*, 1997, vol. 83, pp. 773–78.
51. J.H. Park and D.S. Kim: *Metall. Mater. Trans. B*, 2005, vol. 36B, pp. 495–502.
52. E. Plöckinger: *J. Iron Steel Inst*., 1973, vol. 211, pp. 533–41.
53. W. Holzgruber, K. Petersen, and P.E. Schneider: *Trans. Int. Vac. Metal. Conf*., 1968, pp. 499–523.
54. W.V. Bielefeldt, A.C.F. Vilela, C.A.M. Moraes, and P.C. Fernandes: *Steel Res. Int*., 2007, vol. 78, pp. 857–62.
55. G. Yang, X. Wang, F. Huang, D. Yang, P. Wei, and X. Hao: *Metall. Mater. Trans. B*, 2015, vol. 46B, pp. 145–54.
56. A.L. Kundu, K.M. Gupt, and P.K. Rao: *Metall. Trans. B*, 1989, vol. 20, pp. 581–94.
57. J. Wikström, K. Nakajima, H. Shibata, A. Tilliander, and P. Jönsson: *Mater. Sci. Eng. A*, 2008, vol. 495, pp. 316–19.
58. B.H. Reis, W.V. Bielefeldt, and A.C.F. Vilela: *ISIJ Int*., 2014, vol. 54, pp. 1584–91.
59. G.V. Pervushin and H. Suito: *ISIJ Int*., 2001, vol. 41, pp. 748–56.
60. J.H. Park: *CALPHAD*, 2011, vol. 35, pp. 455–62.
61. J.S. Park, C. Lee, and J.H. Park: *Metall. Mater. Trans. B*, 2012, vol. 43B, pp. 1550–64.
62. C.B. Shi, W.T. Yu, Q.T. Zhu, and J. Li: unpublished research, 2016.